High performance field effect transistors based on αP and βP

E. Montes and U. Schwingenschlögl*

King Abdullah University of Science and Technology (KAUST),

Physical Sciences and Engineering (PSE), Thuwal 23955-6900, Saudi Arabia

Abstract

We investigate the electronic properties of black and blue phosphorus nanoribbons, which enables us to propose junction-free field effect transistors that comprise metallic armchair nanoribbons as electrodes and, in between, a semiconducting zigzag nanoribbon as channel material (cut out of a single sheet of monolayer black or blue phosphorus). Using first principles calculations and the non-equilibrium Green's function method, we characterize the proposed field effect transistors. It turns out that it is possible to achieve outstanding performance, with high on/off ratios, low subthreshold swings, and high transconductances.

* udo.schwingenschlogl@kaust.edu.sa

I. INTRODUCTION

As the miniaturization of electronic elements, such as field effect transistors (FETs), is approaching the physical and geometrical limits, two-dimensional crystalline compounds including graphene, monolayer transition metal dichalcogenides, and phosphorene are attracting considerable attention. Various novel properties have been discovered in these materials that differ fundamentally from those of the bulk counterparts, see for instance Refs. [1–5]. Graphene is known for its low effective mass and ultra-high carrier mobility of up to $\sim 10^5$ $\mathrm{cm^2V^{-1}s^{-1}}$. However, the absence of a band gap limits its applications in electronic devices, and makes it difficult to achieve a high on/off ratio in FETs [6]. Being the prototypical example of a two-dimensional transition metal dichalcogenide, monolayer MoS_2, on the other hand, possesses a large direct band gap (1.8 eV) and provides a relatively high on/off ratio [7, 8]. However, the carrier mobility is limited to $\sim 10^2$ $\mathrm{cm^2V^{-1}s^{-1}}$ [9]. The transport properties of phosphorene fall somewhere in between those of graphene and the monolayer transition metal dichalcogenides. In particular, for few-layer phosphorene FETs band gaps of 0.3 eV to 2.0 eV, mobilities of $\sim 10^3$ $\mathrm{cm^2V^{-1}s^{-1}}$, and on/off ratios of $\sim 10^5$ have been reported [10, 11]. Further device applications based on phosphorene have been discussed in Refs. [12–14].

Phosphorene (derived from black phosphorus; αP) is a two-dimensional material that can be mechanically exfoliated similar to graphene [15]. It shares with graphene the honeycomb lattice but is characterized by a distinct structural anisotropy that is clearly reflected by its electronic states [16, 17]. Dislocations of P atoms can convert the puckered structure of αP into a buckled structure with hexagonal unit cell, giving rise to another two-dimensional allotrope (derived from blue phosphorus; βP) [18]. Based on first principles calculations, βP is as stable as αP, but is predicted to have very different electronic properties. While αP has a direct band gap of ~ 1 eV at the Γ point, the ~ 2 eV band gap of βP is indirect. The electronic states of both materials can be easily modulated by employing axial strain [16, 18]. It may be possible to mechanically exfoliate βP from the bulk compound, while so far it only has been synthesized by molecular beam epitaxial growth on Au(111) substrate [19]. Both αP and βP have great potential in applications due to their extraordinary electronic and thermal transport characteristics [20].

In order to engineer nanostructured FETs a series of strategies has been applied in the

past [21–23], including the use of nanotubes and nanoribbons [24–26]. Because of quantum confinement and unique edge effects, nanoribbons exhibit many exploitable features, in particular from the electrical, optical and magnetic point of view [27, 28]. Nanoribbons of αP can be both metallic and semiconducting, depending on their crystallographic direction and the functionalization of the edges [29–31]. The electronic transport in metallic αP nanoribbons has been investigated theoretically, finding a robust negative differential resistance [32]. On the other hand, both armchair and zigzag βP nanoribbons are semiconducting, while the nature of the band gap (direct or indirect) is different [33, 34].

In order to establish the properties of αP and βP nanoribbons we study in this paper in a first step their electronic structure. In a second step we propose a FET design based on connected armchair and zigzag nanoribbons cut out of a single sheet of αP or βP, which ensures atomically perfect junctions. We then characterize the performance of such devices by means of transport calculations using the non-equilibrium Green's function method.

II. METHODS

Our first principles calculations are based on density functional theory as implemented in the SIESTA code [36, 37]. All structures are fully relaxed until the Hellman-Feynman forces have declined to less than 0.02 eV/Å. We employ double zeta plus polarization basis sets, describe the core electrons by norm-conserving Troullier-Martins pseudopotentials [38], and use for the exchange correlation functional the generalized gradient approximation. The reciprocal space is sampled on a Monkhorst-Pack $1 \times 1 \times 10$ k-mesh and the real space mesh refers to an energy cutoff of 200 Ry.

Electron transport calculations are performed using the non-equilibrium Green's function method (SMEAGOL package [39, 40]). Semi-infinite electrodes connected to the central scattering region give rise to self-energies $\Sigma_{L,R}(E)$. The transmission through the scattering region is described by the transmission coefficient

$$T(E) = \mathrm{Tr}[G_C(E)\Gamma_L(E)G_C^{\dagger}(E)\Gamma_R(E)],$$

where $G_C(E)$ is the retarded Green's function of the central scattering region and $\Gamma_{L,R}(E) = i[\Sigma_{L,R}(E) - \Sigma_{L,R}{}^{\dagger}(E)]$. For a voltage V_{bias} applied to the electrodes, the current is obtained

from the Landauer equation

$$I(V_{\rm bias}) = \frac{2e}{h}\int_{-\infty}^{\infty}[f(E-\mu_L) - f(E-\mu_R)]\,T(E,V_{\rm bias})\,dE,$$

with $\mu_{L/R}$ being the chemical potential of the left/right electrode and f the Fermi distribution function. A square-shaped uniform potential gate is added next to the center of the scattering region. The gate charge density enters the calculation of the electrostatic potential to model a FET geometry.

III. ZIGZAG AND ARMCHAIR NANORIBBONS

In Fig. 1 we show side and front views of αP and βP nanoribbons, different colors indicating the puckering and buckling of the structures. Band structures obtained for pristine αP and βP nanoribbons of width 14.9 Å and 20.4 Å, respectively, are presented in Fig. 2. The armchair nanoribbons turn out to be semiconducting and the zigzag nanoribbons to be metallic. On the right hand side of Fig. 2 we show for the zigzag nanoribbons the charge density obtained for the energy range from -0.2 eV to 0.2 eV. Free carriers are primarily found on the edge P atoms. It is therefore clear that edge functionalization will play a critical role for the electronic properties of these nanoribbons. Indeed, in Refs. [29, 30] it has been demonstrated that zigzag αP nanoribbons are semiconducting (H, OH, F and Cl) or metallic (S, Se and O) depending to the chemical species attached to the edges. Furthermore, Refs. [33, 34] have found band gaps for H terminated armchair and zigzag βP nanoribbons.

We functionalize the edges of our nanoribbons with O due to its high reactivity. The band structures presented in Fig. 3 reveal no influence of the O functionalization on the fact that all armchair nanoribbons are semiconducting and all zigzag nanoribbons are metallic.

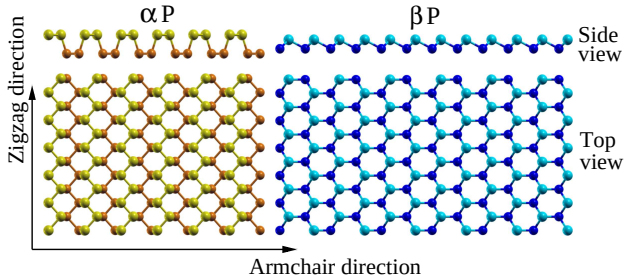

FIG. 1. Crystallographic directions in αP and βP nanoribbons. Different colors are used to indicate the puckering and buckling.

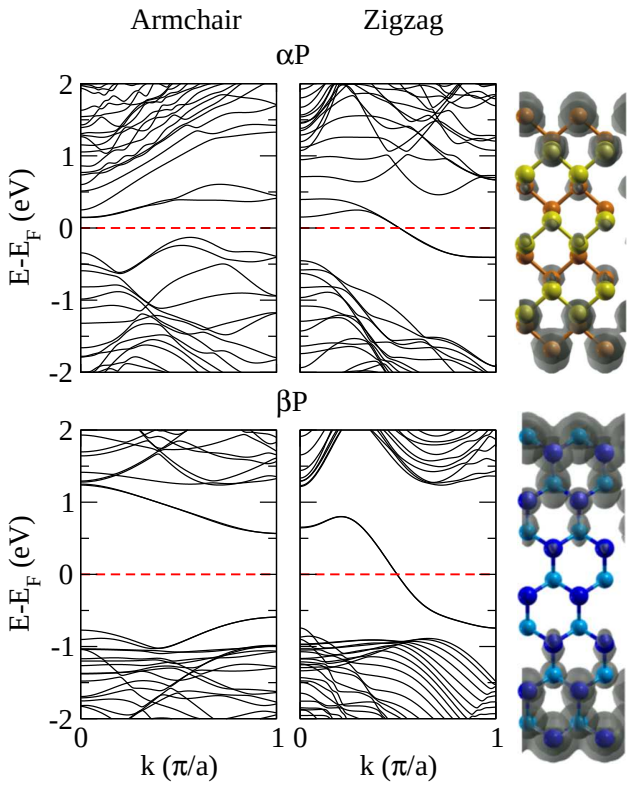

FIG. 2. Band structures of pristine αP and βP nanoribbons. The right hand side shows the charge density of the metallic zigzag nanoribbons for the energy range from -0.2 eV to 0.2 eV (isovalue 0.01 electrons/Å^3).

The charge density of the zigzag nanoribbons for the energy range from -0.2 eV to 0.2 eV is shown on the right hand side of Fig. 3. Free carriers are found for both the edge P and O atoms. We have checked that the semiconducting or metallic character does not depend on the width of the nanoribbon, in the range from 18.2 Å to 43.0 Å for αP and from 14.9 Å to 59.5 Å for βP.

IV. NANORIBBON FET

The different electronic characters of the αP and βP nanoribbons give rise to ideal platforms for engineering FETs. We generate a junction between metallic and semiconducting domains by means of a spatial pattern that combines O-functionalized armchair and zigzag nanoribbons, as shown in Fig. 4. Techniques for fabricating nanoribbons of complex shape are well established for graphene and are transferable to other two-dimensional materials [35].

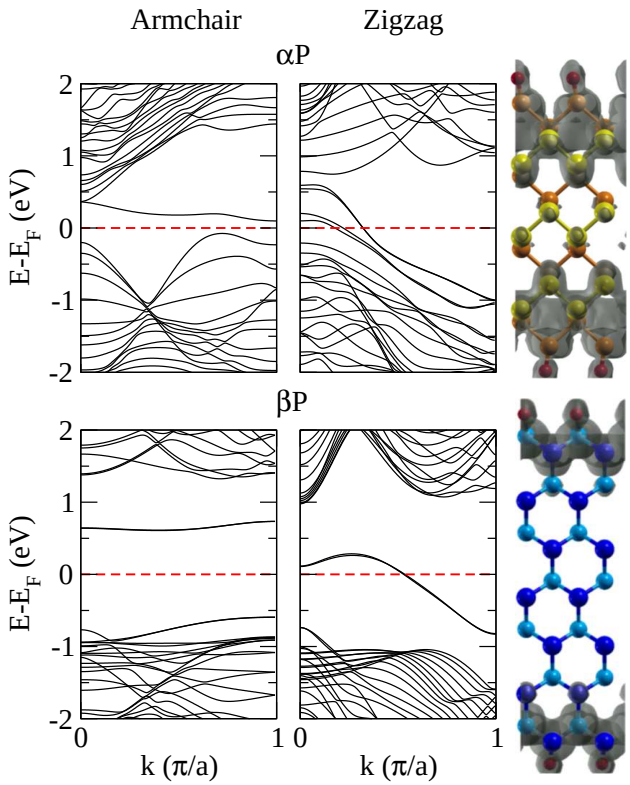

FIG. 3. Band structures of O-functionalized αP and βP nanoribbons. The right hand side shows the charge density of the metallic zigzag nanoribbons for the energy range from -0.2 eV to 0.2 eV (isovalue 0.01 electrons/Å^3).

The chosen setup has several advantages from the engineering point of view. First, junctions between nanoribbons of different chirality do not interrupt the structure, which is impossible to achieve when electrodes of another material are used, since there will always be lattice mismatch. Second, going beyond the structural stability aspect, it is generally difficult to fabricate good contacts to a nanomaterial, resulting in high resistance often combined with a small contact area. In our setup, on the other hand, the continuous metal-semiconductor junction minimizes the contact resistance. Third, controlled doping on the nanoscale is a huge challenge, whereas the edges of nanoribbons provide active sites for dopant atoms to interact with. We note that the electrodes in practice will have to be contacted by normal metals, however, this metal-metal resistance is not critical against the semiconductor-metal resistance.

In order to explore the potential of the proposed FETs, we first address zero-bias electron transport calculations. In Fig. 5 we present the transmission coefficient as a function of the

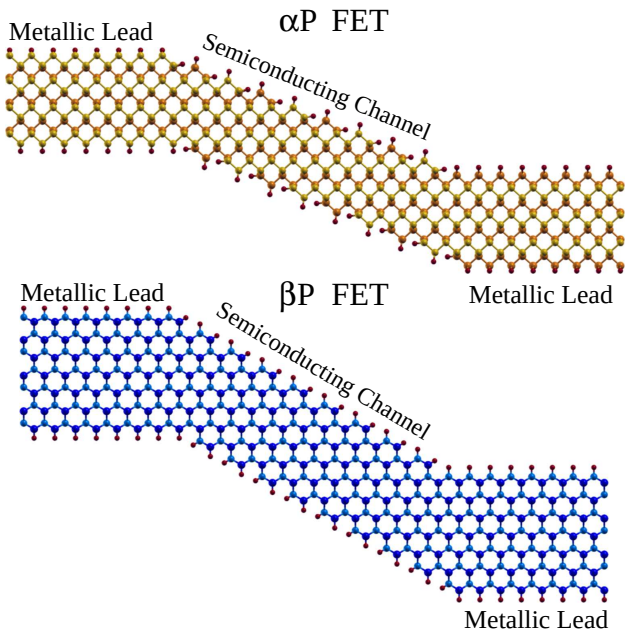

FIG. 4. Schematics of αP and βP FETs, composed of O-functionalized semiconducting zigzag and metallic armchair nanoribbons.

energy for channel widths of 14.9 Å (αP) and 20.4 Å (βP) and channel lengths of 32.5 Å (αP) and 30.1 Å (βP). The overall behavior is similar, with a wide transport gap that represents the armchair semiconducting channel (low resistance of contacts to electrodes). For analyzing the dominant contributions to the transmission, we calculate the eigenchannels by diagonalizing the transmission matrix. For the states contributing most to the transmission (largest eigenvalue) we plot the eigenfunctions originating from the left electrode at the valence band maximum, see the right hand side of Fig. 5. The transmission eigenfunctions extend over the whole semiconducting channel (tunneling regime), while in the electrodes they are localized on the edges as here the metallic nanoribbons provide free carriers. An exception are thin nanoribbons, see for example the αP FET in Fig. 5, where the whole left electrode is covered. We note that the corresponding eigenfunctions originating from the right electrode behave equivalently, as expected from the symmetry of the system [41].

Figure 6 shows typical I-$V_{\rm gate}$ characteristics of the αP and βP FETs, for small $V_{\rm bias}$ = 0.002 V. The curves are close to the symmetric behavior of ambipolar transistors. The on-current is found to be 7×10^{-4} μA in both cases, while the off-current (minimum leakage current) is 3×10^{-6} μA for the αP FET and 2×10^{-6} μA for the βP FET. These values result in high on/off ratios of 233 for the αP FET and 350 for the βP FET, reflecting

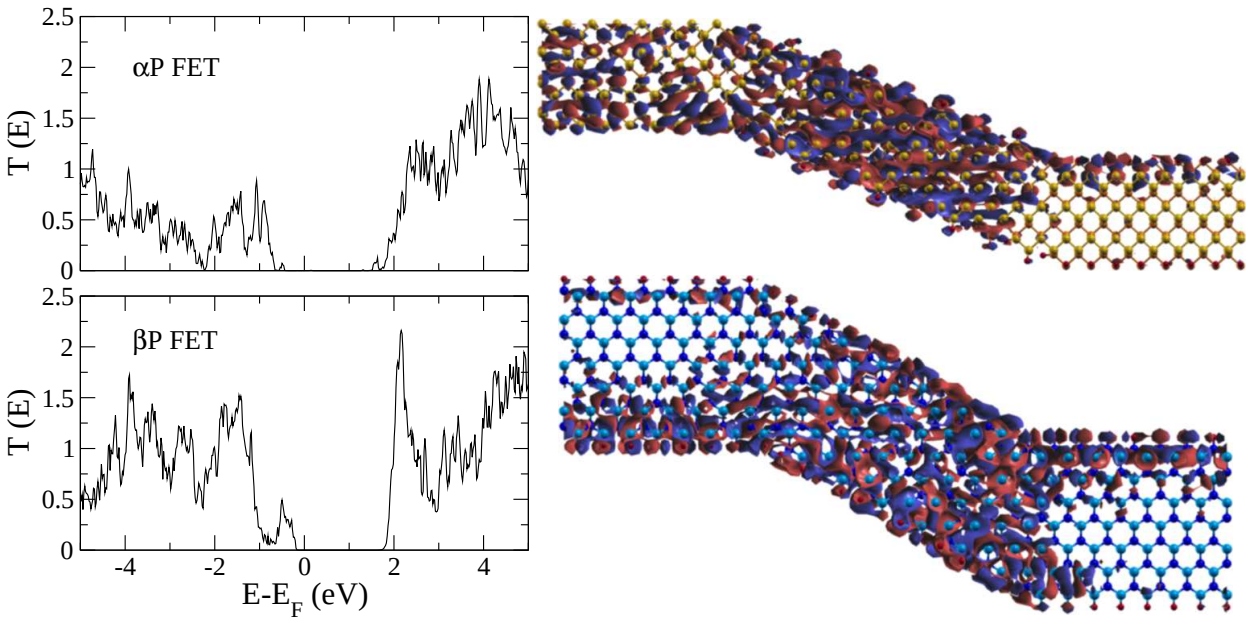

FIG. 5. Transmission coefficients of the αP and βP FETs. The right hand side shows for the states contributing most to the transmission the eigenfunctions originating from the left electrode at the valence band maximum (isovalue 0.001/Å^3).

the atomically perfect junctions between the metallic and semiconducting nanoribbons (low contact resistance). The lower panels of Fig. 6 show the I-$V_{\rm bias}$ characteristics for different values of $V_{\rm gate}$. We observe the typical power-law behavior of tunneling transport, which gradually changes into an Ohmic behavior when $V_{\rm gate}$ increases. Significant variations of the I-$V_{\rm bias}$ characteristics as a function of $V_{\rm gate}$ indicate that the transport properties of the proposed FETs can be effectively modulated.

For further characterization of the FETs we calculate the transconductance $(dI/dV_{\rm gate})/L$, where L is the channel length, using the highest calculated $V_{\rm bias}$ (2 V) as approximation for the point of current saturation. The higher the transconductance the higher is the amplification that the device is capable to deliver. For αP and βP FETs with channel lengths of 32.5 Å and 30.1 Å, for example (the dependence on the channel length is small), we obtain transconductances of 11.2 kS/m and 9.3 kS/m, respectively, which clearly exceed the best values of ~ 7 kS/m obtained experimentally for carbon nanotube FETs [42, 43]. The switching behavior of a FET can be assessed in terms of the subthreshold swing $(d(\log I)/dV_{\rm gate})^{-1}$, small values being desirable for low power consumption. We obtain values of 70.5 mV/decade and 63.9 mV/decade, respectively, i.e., close to the theoretical limit of $(k_BT/e)/\ln 10 \sim 60$

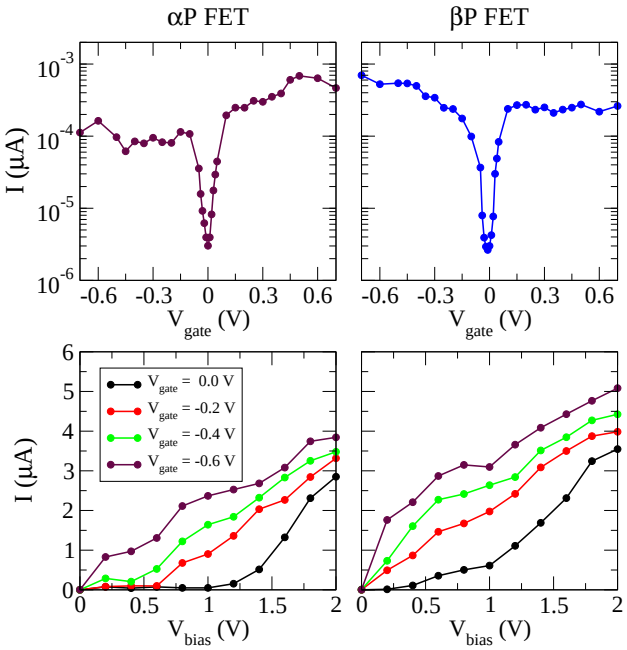

FIG. 6. Comparison of αP and βP FETs: I-$V_{\rm gate}$ characteristics for $V_{\rm bias} = 0.002$ V and I-$V_{\rm bias}$ characteristics for different values of $V_{\rm gate}$.

mV/decade. The values compare well with those of carbon nanotube FETs and commercial silicon-based FETs (70 mV/decade to 80 mV/decade) [42, 43]. Few-layer phosphorene FETs achieve much worse subthreshold swings [10].

V. CONCLUSIONS

We have performed band structure calculations to study the electronic properties of αP and βP nanoribbons. It turns out that both these two-dimensional materials give rise to promising platforms for engineering *junction-free FETs* based on semiconducting zigzag nanoribbons connected to metallic armchair nanoribbons as electrodes. Electronic transport calculations have been used to elucidate trends in the performance of the proposed FETs with respect to key operational parameters. It is possible to achieve simultaneously high on/off ratios (reflecting the atomically perfect junctions), low subthreshold swings close to the theoretical limit, and high transconductances. We find that βP FETs perform slightly better than αP FETs, since the subthreshold swing is smaller and the transconductance higher. Importantly, the performance is expected to be well tunable by means of controlled functionalization of the nanoribbon edges. The proposed devices can be naturally integrated

in circuit architectures fabricated by nanopatterning.

VI. ACKNOWLEDGMENT

The research reported in this publication was supported by funding from King Abdullah University of Science and Technology (KAUST).

---

[1] A. H. Castro Neto, F. Guinea, N. M. R. Peres, K. S. Novoselov and A. K. Geim, Rev. Mod. Phys. **81**, 109 (2009).

[2] Q. H. Wang, K. Kalantar-Zhadeh, A. Kis, J. N. Coleman and M. S. Strano, Nat. Nanotechnol. **7**, 699 (2012).

[3] Q. Yue, S. Chang, J. Kang, X. Zhang, Z. Shao, Q. Qin and J. Li, J. Phys.: Condens. Matter **24**, 335501 (2012).

[4] H. O. H. Churchill and P. Jarrillo-Herrero, Nat. Nanotechnol. **9**, 330 (2014).

[5] Y. Jing, X. Zhang and Z. Zhou, WIREs Comput. Mol. Sci. **6**, 5 (2016).

[6] K. S. Novoselov, A. K. Geim, S. V. Morozov, D. Jiang, M. I. Katsnelson, I. V. Grigorieva, S. V. Dubonos and A. A. Firsov, Nature **438**, 197 (2005).

[7] B. Radisavljevic, A. Radenovic, J. Brivio, V. Giacometti and A. Kis, Nat. Nanotechnol. **6**, 147 (2011).

[8] W. Wu, D. De, S.-C. Chang, Y. Wang, H. Peng, J. Bao and S.-S. Pei, Appl. Phys. Lett. **102**, 142106 (2013).

[9] K. F. Mak, C. Lee, J. Hone, J. Shan and T. F. Heinz, Phys. Rev. Lett. **105**, 136805 (2010).

[10] L. Li, Y. Yu, G. J. Ye, Q. Ge, X. Ou, H. Wu, D. Feng, X. H. Chen and Y. Zhang, Nat. Nanotechnol. **9**, 372 (2014).

[11] X. Ling, H. Wang, S. Huang, F. Xia and M. S. Dresselhaus, Proc. Natl. Acad. Sci. USA **112**, 4523 (2015).

[12] Y. Zhou, M. Zhang, Z. Guo, L. Miao, S.-T. Han, Z. Wang, X. Zhang, H. Zhang and Z. Peng, Mater. Horiz. **4**, 997 (2017).

[13] S. C. Dhanabalan, J. S. Ponraj, Z. Guo, S. Li, Q. Bao, and H. Zhang, Adv. Sci. **4**, 1600305 (2017).

[14] Z. Guo, S. Chen, Z. Wang, Z. Yang, F. Liu, Y. Xu, J. Wang, Y. Yi, H. Zhang, L. Liao, P. K. Chu and X.-F. Yu, Adv. Mater. **29**, 1703811 (2017).

[15] F. Xia, H. Wang and Y. Jia, Nat. Commun. **5**, 458 (2014).

[16] H. Liu, A. T. Neal, Z. Zhu, Z. Luo, X. Xu, D. Tománek and P. D. Ye, ACS Nano **8**, 4033 (2014).

[17] H. Liu, Y. Du, Y. Deng and P. D. Ye, Chem. Soc. Rev. **44**, 2732 (2015).

[18] Z. Zhu and D. Tománek, Phys. Rev. Lett. **112**, 176802 (2014).

[19] J. L. Zhang, S. Zhao, C. Han, Z. Wang, S. Zhong, S. Sun, R. Guo, X. Zhou, C. D. Gu, K. D. Yuan, Z. Li and W. Chen, Nano Lett. **16**, 4903 (2016).

[20] A. Jain and A. J. H. MacGaughey, Sci. Rep. **5**, 8501 (2015).

[21] C. W. Zhou, J. Kong and H. J. Dai, Appl. Phys. Lett. **76**, 1597 (2000).

[22] K. S. Novoselov, A. K. Geim, S. V. Morozov, D. Jiang, Y. Zhang, S. V. Dubonos, I. V. Grigorieva and A. A. Firsov, Science **306**, 666 (2004).

[23] G.-H. Lee, Y.-J. Yu, X. Cui, N. Petrone, C.-H. Lee, M. S. Choi, D.-Y. Lee, C. Lee, W. J. Yoo, K. Watanabe, T. Taniguchi, C. Nuckolls, P. Kim and J. Hone, ACS Nano **7**, 7931 (2013).

[24] A. D. Franklin, M. Luisier, S.-J. Han, G. Tulevski, C. M. Breslin, L. Gignac, M. S. Lundstrom and W. Haensch, Nano Lett. **12**, 758 (2012).

[25] P. B. Bennett, Z. Pedramrazi, A. Madani, Y.-C. Chen, D. G. de Oteyza, C. Chen, F. R. Fischer, M. F. Crommie and J. Bokor, Appl. Phys. Lett. **103**, 253114 (2013).

[26] T. Roy, M. Tosun, J. S. Kang, A. B. Sachid, S. B. Desai, M. Hettick, C. C. Hu and A. Javey, ACS Nano **8**, 6259 (2014).

[27] M. Terrones, A. R. Botello-Méndez, J. Campos-Delgado, F. López-Urías, Y. I. Vega-Cantú, F. J. Rodríguez-Macías, A. L. Elías, E. Muñoz-Sandoval, A. G. Cano-Márquez, J.-C. Charlier, H. Terrones, Nano Today **5**, 351 (2010).

[28] J. M. Marmolejo-Tejada and J. Velasco-Medina, Microelectron. J. **48**, 18 (2016).

[29] H. Guo, N. Lu, J. Dai, X. Wu and X. C. Zeng, J. Phys. Chem. C **118**, 14051 (2014).

[30] W. Li, G. Zhang and Y.-W. Zhang, J. Phys. Chem. C **118**, 22368 (2014).

[31] X. Peng, A. Copple and Q. Wei, J. Appl. Phys. **116**, 144301 (2014).

[32] C. Zhang, G. Xiang, M. Lan, Z. Tang, L. Deng and X. Zhang, RSC Adv. **5**, 40358 (2015).

[33] J. Xie, M. S. Si, D. Z. Yang, Z. Y. Zhang and D. S. Xue, J. Appl. Phys. **116**, 073704 (2014).

[34] J. Xiao, M. Long, C.-S. Deng, J. He, L.-L. Cui and H. Xu, J. Phys. Chem. C **120**, 4638 (2016).

[35] M. Y. Han, B. Özyilmaz, Y. Zhang, and P. Kim, Phys. Rev. Lett. **98**, 206805 (2007).

[36] D. Sánchez-Portal, P. Ordejón, E. Artacho and J. M. Soler, Int. J. Quantum Chem. **65**, 453 (1997).

[37] J. M. Soler, E. Artacho, J. D. Gale, A. García, J. Junquera, P. Ordejón and D. Sánchez-Portal, J. Phys.: Condens. Matter **14**, 2745 (2002).

[38] N. Troullier and J. L. Martins, Phys. Rev. B **43**, 1993 (1991).

[39] A. R. Rocha, V. M. García-Suarez, S. W. Báiley, C. J. Lambert, J. Ferrer and S. Sanvito, Nat. Mater. **4**, 335 (2005).

[40] I. Rungger and S. Sanvito, Phys. Rev. B **78**, 035407 (2008).

[41] M. Paulsson and M. Brandbyge, Phys. Rev. B **76**, 115117 (2007).

[42] A. Javey, H. Kim, M. Brink, Q. Wang, A. Ural, J. Guo, P. Mcintyre, P. Mceuen, M. Lundstrom and H. Dai, Nat. Mater. **1**, 241 (2002).

[43] A. Javey, J. Guo, D. B. Farmer, Q. Wang, D. Wang, R. G. Gordon, M. Lundstrom and H. Dai, Nano Lett. **4**, 447 (2004).